

A UNIFIED EMPIRICAL MODEL FOR INFRARED GALAXY COUNTS BASED ON THE OBSERVED PHYSICAL EVOLUTION OF DISTANT GALAXIES

MATTHIEU BÉTHERMIN¹, EMANUELE DADDI¹, GEORGIOS MAGDIS², MARK T. SARGENT¹, YASHAR HEZAVEH³, DAVID ELBAZ¹, DAMIEN LE BORGNE^{4,5}, JAMES MULLANEY¹, MAURILIO PANNELLA¹, VÉRONIQUE BUAT⁶, VASSILIS CHARMANDARIS⁷, GUILAINE LAGACHE⁸, AND DOUGLAS SCOTT⁹

ApJ Letters in press

Abstract

We reproduce the mid-infrared to radio galaxy counts with a new empirical model based on our current understanding of the evolution of main-sequence (MS) and starburst (SB) galaxies. We rely on a simple Spectral Energy Distribution (SED) library based on *Herschel* observations: a single SED for the MS and another one for SB, getting warmer with redshift. Our model is able to reproduce recent measurements of galaxy counts performed with *Herschel*, including counts per redshift slice. This agreement demonstrates the power of our 2 Star-Formation Modes (2SFM) decomposition for describing the statistical properties of infrared sources and their evolution with cosmic time. We discuss the relative contribution of MS and SB galaxies to the number counts at various wavelengths and flux densities. We also show that MS galaxies are responsible for a bump in the 1.4 GHz radio counts around 50 μ Jy. Material of the model (predictions, SED library, mock catalogs...) is available online^a.

Subject headings: galaxies: statistics — galaxies: evolution — galaxies: star formation — infrared: galaxies — submillimeter: galaxies

1. INTRODUCTION

Recent observational studies have shown that two distinct star-forming (SF) mechanisms are required to describe the SF galaxy population. The so-called SF main sequence (MS) is composed of secularly-evolving galaxies that display a tight correlation between stellar mass (M_*) and star formation rate (SFR) at a given redshift (e.g. Elbaz et al. 2007; Noeske et al. 2007; Daddi et al. 2007). This population accounts for $\sim 85\%$ of the star formation rate density (SFRD) in the Universe (Rodighiero et al. 2011; Sargent et al. 2012) at $z < 2$. The rest of the star-formation budget is provided by starbursts (SB), i.e. galaxies with very high specific star formation rates (sSFR=SFR/ M_*), probably induced by recent mergers (e.g. Elbaz et al. 2011; Rodighiero et al. 2011). Recently, Sargent et al. (2012, S12 hereafter) showed that infrared (IR) luminosity functions (LF) can be reproduced by jointly considering the mass function of SF galaxies (SFMF), the evolution of the sSFR of MS galaxies, and its distribution at fixed M_* , with a separate contribution from MS and SB galaxies.

Wavelength-dependent galaxy number counts are an additional, important constraint for evolutionary models of infrared galaxies. While purely semi-analytical models (e.g. Lacey et al. 2010; Somerville et al. 2012) struggle to reproduce infrared (IR) number counts, phenomenological or hybrid models (e.g. Béthermin et al. 2011; Gruppioni et al. 2011; Rahmati & van der Werf 2011; Lapi et al. 2011) fare better but are in general descriptive and use an evolution of the luminosity function which is not motivated by physical principles. However, these recent models which reproduce the total counts passably, are excluded at $>3\sigma$ by the recent *Herschel* measurements of counts per redshift slice (Berta et al. 2011; Béthermin et al. 2012b). This shows how important redshift-dependent constraints are to accurately model the evolution of galaxies, and motivates the development of a new generation of models.

We present a new model of IR galaxy counts which builds on the 2-Star-Formation-Mode framework (2SFM) S12 introduced. This fiducial model is intuitive and based on our current observational knowledge of the evolution of MS and SB galaxies. All model parameters are constrained by external datasets and require no additional fine-tuning. We assume a Salpeter initial mass function and a *WMAP-7* cosmology.

2. MAIN INGREDIENTS

Our model is based on four main ingredients, which are sufficient to reach a good agreement with IR source counts (see Sect. 4 and grey line Fig. 3):

- evolution of the MS with redshift,
- decomposition of the sSFR distribution at fixed M_* into MS and SB modes,
- evolution of the SFMF with redshift,

¹ Laboratoire AIM-Paris-Saclay, CEA/DSM/Irfu - CNRS - Université Paris Diderot, CEA-Saclay, Orme des Merisiers, F-91191 Gif-sur-Yvette, France, Email: matthieu.bethermin@cea.fr

² Department of Physics, University of Oxford, Keble Road, Oxford OX1 3RH, UK

³ Department of Physics, McGill University, 3600 Rue University, Montreal, Quebec H3A 2T8, Canada

⁴ UPMC Univ. Paris 06, UMR7095, Institut d'Astrophysique de Paris, 75014 Paris, France

⁵ CNRS, UMR7095, Institut d'Astrophysique de Paris, 75014 Paris, France

⁶ Laboratoire d'Astrophysique de Marseille, OAMP, Université Aix-Marseille, CNRS, 38 rue Frédéric Joliot-Curie, 13388 Marseille Cedex 13, France

⁷ Department of Physics & Institute of Theoretical and Computation Physics, University of Crete, 71003 Heraklion, Greece

⁸ Institut d'Astrophysique Spatiale (IAS), bâtiment 121, Université Paris-Sud 11 and CNRS (UMR 8617), 91405 Orsay, France

⁹ Department of Physics & Astronomy, University of British Columbia, 6224 Agricultural Road, Vancouver, BC V6T 1Z1, Canada

^a at <http://irfu-i.cea.fr/Pisp/matthieu.bethermin/>

- Spectral Energy Distribution (SED) libraries for MS and SB galaxies.

Additional ingredients, which are of lesser importance, are presented in Sect. 3.

2.1. SFR distribution

A key ingredient of the S12 approach is the probability distribution of sSFR at fixed M_\star for SF galaxies based on observations presented in Rodighiero et al. (2011). It is parametrized as a double log-normal decomposition of MS and SB:

$$p(\log(\text{sSFR})) \propto \exp\left(-\frac{(\log(\text{sSFR}) - \log(\text{sSFR}_{MS}))^2}{2\sigma_{MS}^2}\right) + r_{SB} \times \exp\left(-\frac{(\log(\text{sSFR}) - \log(\text{sSFR}_{MS}) - B_{SB})^2}{2\sigma_{SB}^2}\right), \quad (1)$$

where σ_{MS} and σ_{SB} are the dispersion in the sSFR of the MS and the SB populations. B_{SB} is the average sSFR-boost for SB galaxies. We assume that these three parameters do not evolve with M_\star and redshift, as suggested by S12 who reproduce the $z \sim 0$ IR LF under these assumptions and with the distribution calibrated at $z \sim 2$ (see Table 1 for parameter values adopted). sSFR_{MS} varies with M_\star and redshift according to

$$\text{sSFR}_{MS}(z, M_\star) = \text{sSFR}_{MS,0} \times \left(\frac{M_\star}{10^{11} M_\odot}\right)^{\beta_{MS}} \times (1 + \min(z, z_{evo}))^{\gamma_{MS}}, \quad (2)$$

where $\text{sSFR}_{MS,0}$ is the sSFR at $z=0$ for $M_\star = 10^{11} M_\odot$ and β_{MS} parametrizes the dependence of sSFR on M_\star . γ_{MS} describes the evolution of the normalization of the MS out to redshift $z_{evo} = 2.5$ where this evolution flattens according to observations (e.g. González et al. 2010). The values of these parameters, chosen based on measurements summarized in Fig. 1bc, are listed in Table 1. S12 also present evidence for a weak redshift evolution of r_{SB} , the relative amplitude of SB sSFR log-normal distribution compared to MS one (or, equivalently, of the relative SB-contribution to the SFRD, see Fig. 1d), in agreement with the model of Hopkins et al. (2010). Here we define the redshift evolution of r_{SB} as:

$$r_{SB}(z) = r_{SB,0} \times (1 + \min(z, z_{SB}))^{\gamma_{SB}}, \quad \text{where } z_{SB} = 1, \quad (3)$$

in order to broadly reproduce the trends suggested by these two studies (see Fig. 1d). The impact of this evolving r_{SB} is negligible, barring a $\sim 20\%$ decrease of $70 \mu\text{m}$ counts compared to a constant r_{SB} .

Another important ingredient of our model is the evolution of the SFMF. Observations are well-described by a Schechter function

$$\phi = \frac{dN}{d\log(M_\star)} = \phi_b(z) \times \left(\frac{M_\star}{M_b}\right)^{-\alpha_{MF}} \times \exp\left(-\frac{M_\star}{M_b}\right) \times \frac{M_\star}{M_b} \ln(10) \quad (4)$$

with a redshift-invariant characteristic mass M_b and faint-end slope α_{MF} , in keeping with Peng et al. (2010). ϕ_b , the characteristic density, is constant between $z=0$ and $z=1$ but decreases at $z > 1$ as

$$\log(\phi_b) = \log(\phi_b)(z < 1) + \gamma_{SFMF}(1 - z). \quad (5)$$

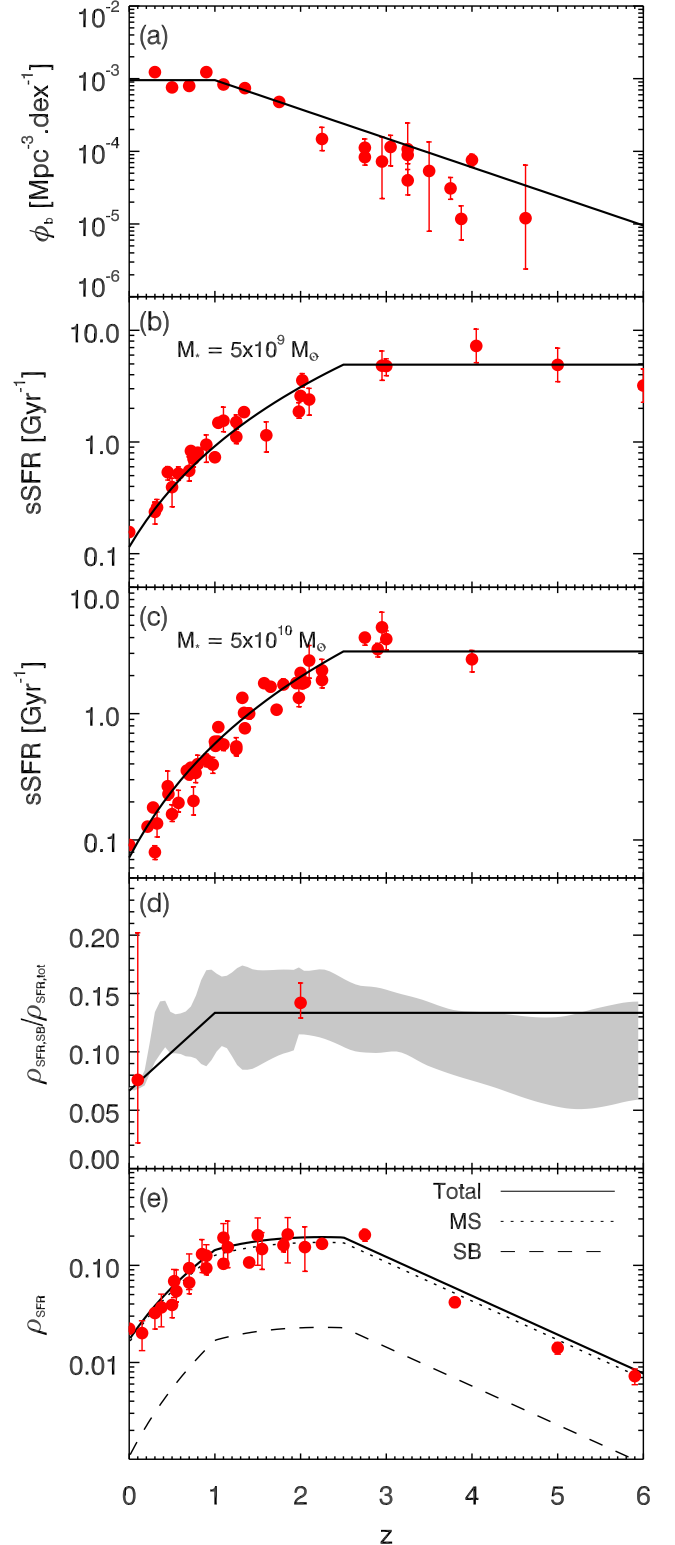


FIG. 1.— Redshift evolution of selected model parameters and derived quantities; model conventions are represented using a solid line; (a) – density at the break of the mass function; (b) – sSFR at $M_\star = 5 \times 10^9 M_\odot$. (c) – sSFR at $M_\star = 5 \times 10^{10} M_\odot$ (data in a, b, and c from a compilation of Sargent et al. in prep.); (d) – contribution of SB to the total star formation rate density (data from S12; grey region from Hopkins et al. 2010). (e) – SFRD. The MS (SB) contribution is represented by a dotted (dashed) line (data: Bouwens et al. (2007), Rodighiero et al. 2011, Magnelli et al. 2011 and Karim et al. 2011).

TABLE 1
SUMMARY OF PARAMETERS OF OUR FIDUCIAL MODEL.

Parameter	Description	Value	Reference
Distribution of sSFR			
B_{SB}	Boost of specific star formation rate in SB (in dex)	0.6	Sargent et al. (2012, hereafter S12)
σ_{MS}	Width of the MS log-normal distribution (in dex)	0.15	S12 value minus 0.05 dex for artificial scatter (Salmi et al. 2012)
σ_{SB}	Width of the SB log-normal distribution (in dex)	0.20	S12 value minus 0.05 dex for artificial scatter (Salmi et al. 2012)
Evolution of the main MS			
$sSFR_{MS,0}$	sSFR on the MS at $z = 0$ and $M_{\star} = 10^{11} M_{\odot}$ (in $\log(\text{yr}^{-1})$)	-10.2	S12 based on a fit of literature data
β_{MS}	Slope of the sSFR- M_{\star} relation at a given redshift	-0.2	Rodighiero et al. (2011) and S12
γ_{MS}	Evolution of the normalization of the MS with redshift	3	compilation of measurements of sSFR (see Fig. 1)
z_{evo}	Redshift where the MS normalization stops to evolve	2.5	compilation of measurements of sSFR (see Fig. 1)
Evolution of the fraction of SB			
$r_{SB,0}$	Relative amplitude of SB log-normal distribution compared to MS	0.012	S12 and Hopkins et al. (2010) (see Fig. 1)
γ_{SB}	Evolution of starburst fraction with redshift	1	S12 and Hopkins et al. (2010) (see Fig. 1)
z_{SB}	Redshift where the starburst fraction stops to evolve	1	S12 and Hopkins et al. (2010) (see Fig. 1)
Star-forming mass function (SFMF) and its evolution			
M_b	Stellar mass at the break of the SFMF (in $\log(M_{\odot})$)	11.20	Ilbert et al. (2010) and Peng et al. (2010)
α	Faint-end slope of the SFMF	1.3	Ilbert et al. (2010) and Peng et al. (2010)
$\phi_b(z < 1)$	Number density at the break of the SFMF at $z < 1$ (in $\log(\text{Mpc}^{-3})$)	-3.02	Sargent et al. (2012) (see Fig. 1)
γ_{SFMF}	Evolution of the density of SFMF at $z > 1$	0.4	Extended from Sargent et al. (2012) (see Fig. 1)
Evolution of SEDs			
$\langle U \rangle_{MS,0}$	Mean radiation field in local MS galaxies	4	Magdis et al. (2012) and Fig. 2
$\gamma_{U,MS}$	Evolution of the radiation field in MS with redshift	1.3	Magdis et al. (2012) and Fig. 2
$z_{(U),MS}$	Redshift where $\langle U \rangle$ in MS flattens	2	Magdis et al. (2012) and Fig. 2
$\langle U \rangle_{SB,0}$	Mean radiation field in local SB galaxies	35	Magdis et al. (2012) and Fig. 2
$\gamma_{U,SB}$	Evolution of the radiation field in SB with redshift	0.4	Magdis et al. (2012) and Fig. 2
$z_{(U),SB}$	Redshift where $\langle U \rangle$ in SB flattens	3.1	Magdis et al. (2012) and Fig. 2
Contribution of AGNs			
A_{AGN}	Normalization of the probability distribution of AGN contribution	0.0025	Aird et al. (2012)
β_{AGN}	Slope of the probability distribution of AGN contribution	-0.7	See Sect. 3

The fiducial values (chosen from Fig. 1a) of the MF-related parameters are also listed in Table 1.

The star formation history implied by our evolutionary formalism is shown in Fig. 1e. The star formation rate density increases from $z=0$ to 1, flattens between $z = 1$ and $z = z_{evo} = 2.5$ and decreases with redshift at $z > z_{evo}$, matching the infrared measurements of Magnelli et al. (2011) and Rodighiero et al. (2011), the radio measurements of Karim et al. (2011), and the optical measurements of Bouwens et al. (2007) at high redshift. The SFMF is quite uncertain at $z > 4$, but this has little impact on the counts. In our model, the SFRD is dominated by MS galaxies at all redshifts.

2.2. SEDs

We use a characteristic IR SED template for MS and SB based on fits of Draine & Li (2007) models to *Herschel* observations of distant galaxies as presented in Magdis et al. (2012, hereafter M12). While conceptually similar to Elbaz et al. (2011), however, our templates evolve with redshift following the finding of M12 that the mean radiation field $\langle U \rangle$ (which correlates with dust temperature) is more intense at high redshift:

$$\langle U \rangle = \langle U \rangle_0 \times (1 + \min(z, z_{(U)}))^{y_U}. \quad (6)$$

Here $\langle U \rangle_0$ is the mean radiation field in local MS galaxies, y_U a parameter determining its evolution with redshift, and $z_{(U)}$ the redshift where $\langle U \rangle$ flattens. This evolution is different in MS and SB galaxies (see Fig. 2 and Table 1). This evolution is caused by the evolution of SF efficiency and metallicity with redshift (M12), and is required to reproduce source

counts. For example, if we used the $z=1$ ($z=0$) MS template for all redshifts, we would overestimate the counts by about a factor of 2 (1) at $70 \mu\text{m}$ and 2 (10) at 1.1 mm. For reference, if we use the MS and SB templates of Elbaz et al. (2011), we overpredict the mm counts by a factor of 10 at all fluxes and underpredict the $100 \mu\text{m}$ counts by $\sim 30\%$. To reproduce the $24 \mu\text{m}$ counts, it is crucial to use distinct SB templates with less mid-IR emission than in MS galaxies. The SEDs of MS and SB galaxies used in our model are shown in Fig. 2. We introduce a relative dispersion on $\langle U \rangle$ of 0.2 dex for both MS and SB (M12), which has little impact on the counts ($< 10\%$), except in the millimeter domain ($+20\%$). In this approach, the increasing mean dust temperature with infrared luminosity (L_{IR}) at a given redshift is caused by a higher fraction of SB galaxies at higher L_{IR} .

3. REFINEMENTS

3.1. Dust attenuation

To reproduce IR number counts we have to link SFR and L_{IR} . For obscured SF galaxies, the bulk of the UV light emitted by young stars is absorbed by dust and re-emitted in the IR ($SFR_{IR}/L_{IR} = K = 1.7 \times 10^{-10} M_{\odot} \text{yr}^{-1} L_{\odot}^{-1}$, Kennicutt 1998). In less massive galaxies, the attenuation is smaller and a significant part of the SF can be detected in UV. The total star formation can then be divided into an uncorrected UV and an IR component ($SFR = SFR_{UV} + SFR_{IR}$). The mean ratio between these two components, r_{1500} , varies with M_{\star} . Here, we apply the relation of Pannella et al. (2009):

$$r_{1500} = 2.5 \log \left(\frac{SFR_{IR}}{SFR_{UV}} \right) = 4.07 \times \log \left(\frac{M_{\star}}{M_{\odot}} \right) - 39.32, \quad (7)$$

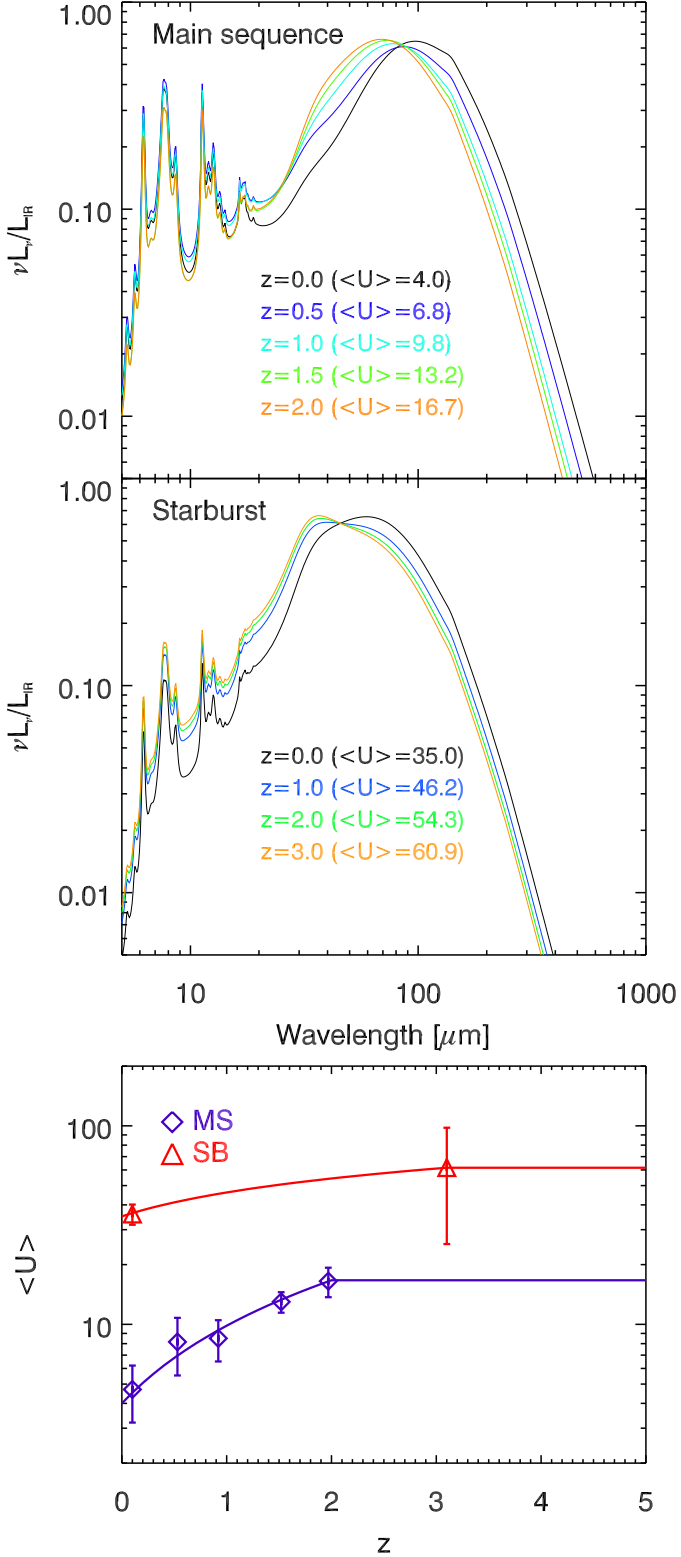


FIG. 2.— SEDs (normalized to have $L_{IR} = 1 L_{\odot}$) for MS (top) and SB (middle) used in our model. Evolution of $\langle U \rangle$ parameter with redshift in MS (blue) and SB (red) galaxies (data from M12).

and assume redshift-invariance, as suggested by Sobral et al. (2012) and Pannella et al. (in prep.). The IR luminosity of the galaxies, L_{IR} is thus given by:

$$L_{IR} = \frac{SFR_{IR}}{K} = \frac{SFR}{K} \times \frac{10^{0.4 \times r_{1500}}}{1 + 10^{0.4 \times r_{1500}}} = \frac{SFR}{K} \times f_{IR}^{SF}(M_{\star}), \quad (8)$$

where $f_{IR}^{SF}(M_{\star}) = SFR_{IR}/SFR$ goes to 0 at low mass and 1 at high mass. This correction implies a flatter IR LF at the faint end as compared to the SFMF at the low-mass end and prevents an excess in the counts at faint flux densities. Although a small part of the IR emission is due to dust heated by old stars, especially at low- z , we consistently reproduce $z = 0 - 2$ IR LF (S12).

3.2. AGN contribution

Active-Galactic-Nucleus (AGN) activity is potentially important when modeling mid-IR counts. We statistically associate an AGN contribution, represented by the average intrinsic SED template of Mullaney et al. (2011), to each galaxy based on its L_{IR} . Aird et al. (2012) showed that the Eddington ratio r_{Edd} (bolometric luminosity L_{bol}^{AGN} over Eddington luminosity) of AGN at $z < 1$ follows a power-law probability distribution function (PDF) with redshift-dependent normalization. Based on the results of Mullaney et al. (2012) – who report a coincident cosmological evolution of the averages of specific black hole (BH) growth (\dot{M}_{BH}/M_{BH} , where M_{BH} is BH mass) and sSFR over $0.5 < z < 2.5$, a fact that implies constant M_{BH}/M_{\star} ratios –, we can express the Aird et al. (2012) results in terms of a distribution of ratios of bolometric luminosities ($r_{AGN} = L_{IR}^{AGN}/L_{IR}^{SF}$) from AGN and SF with redshift-independent normalization:

$$p(r_{Edd}) = C(z) \times r_{Edd}^{\beta_{AGN}} \rightarrow p(r_{AGN}) = A_{AGN} \times r_{AGN}^{\beta_{AGN}}, \quad (9)$$

where we recall that

$$\frac{\dot{M}_{BH}}{M_{BH}} \propto \frac{L_{bol}^{AGN}}{M_{\star}} \propto \frac{L_{IR}^{AGN}}{(L_{IR}^{SF})^{1+\beta_{MS}}} \approx \frac{L_{IR}^{AGN}}{L_{IR}^{SF}}. \quad (10)$$

The last step uses the M_{\star} -SFR correlation. $\beta_{AGN} = -0.7$ comes from Aird et al. (2012). A_{AGN} is based on the normalization of the Aird et al. (2012) relation and includes a scaling factor for the conversion between r_{Edd} and r_{AGN} PDFs. This scaling relation assumes a mean ratio between black hole and stellar mass of 0.0015 (Mullaney et al. 2012), plus a mean ratio between L_{IR}^{AGN} and L_{bol}^{AGN} calibrated from Mullaney et al. (2011), Lutz et al. (2004) and Vasudevan & Fabian (2007). In order to normalize this PDF, we place a cut at $\lambda_{Edd} = 1$ and choose a lower bound such that $\int p(r_{AGN}) dr_{AGN} = 1$. We emphasize that Eq. 9 implies a correlation between AGN and SF activity only in an average sense, while preserving a large dispersion for individual objects consistent with observations. Full details of our AGN-treatment will be presented in a future paper. The AGN contribution is significant ($> 10\%$) only at $24 \mu\text{m}$ above 3 mJy (see Fig. 3) and negligible at longer wavelengths ($< 2\%$).

3.3. Magnification caused by strong lensing

Having computed the IR LF, split into MS and SB contribution as in S12, we include the effect of the strong ($\mu > 2$)

lensing (Negrello et al. 2007, 2010) on these two LFs:

$$\left. \frac{d^2 N}{d \log L_{IR} dV} \right|_{\text{lensed}} = \int_{\mu=2}^{\infty} \frac{dP(\mu, z)}{d \log \mu} \left. \frac{d^2 N}{d \log L_{IR} dV} \right|_{\text{initial}} d \log \mu, \quad (11)$$

where μ is the magnification, $\frac{dP}{d \log \mu}$ the magnification PDF in the Hezaveh & Holder (2011) model, and $\frac{d^2 N}{d \log L_{IR} dV}$ the luminosity function. These lensed sources contribute $\sim 20\%$ to (sub-)mm counts around 100 mJy.

4. RESULTS

Number counts are computed according to:

$$\begin{aligned} \frac{d^2 N}{dS dz}(S, z, \lambda) = & \sum_{\text{type} = \{\text{MS}, \text{SB}\}} \int_{\langle U \rangle} \int_{r_{AGN}} dr_{AGN} d\langle U \rangle \\ & \times \frac{d^2 N_{\text{type}}}{dL_{IR} dV}(z, L_{IR}(S, \text{type}, \langle U \rangle, z)) \\ & \times \frac{1 L_{\odot}}{S_{\text{norm}}^{\text{type}, \langle U \rangle}(z, \lambda) + r_{AGN} \times S_{\text{norm}}^{\text{AGN}}(z, \lambda)} \frac{dV}{dz} p(r_{AGN}) p(\langle U \rangle | z, \text{type}) \end{aligned} \quad (12)$$

Here $S_{\text{norm}}^{\text{type}, \langle U \rangle}$ is the flux of a $L_{IR} = 1 L_{\odot}$ source of a given type (MS or SB) and a given $\langle U \rangle$ in a given filter. $S_{\text{norm}}^{\text{AGN}}$ is the same quantity, computed using the Mullaney et al. (2011) AGN template. Note that the filter shape is taken into account for the calculation of S_{ν} . $p(r_{AGN})$ is provided by Eq. 9 and $p(\langle U \rangle)$ is a log-normal distribution with a width of 0.2 dex (see Sect. 2).

We compare the predictions of our model with measurements of differential galaxy counts from $24 \mu\text{m}$ to 1.1 mm (see Fig. 3). *Spitzer* and *Herschel* counts are well reproduced, showing the effectiveness of our new approach. Note, however, a 10-20% ($\sim 2\sigma$) excess at $24 \mu\text{m}$ between 400 μJy and 2 mJy, and a $\sim 20\%$ ($\sim 2\sigma$) excess at the faint-end at 70 and 160 μm ($< 1 \text{ mJy}$ and $< 5 \text{ mJy}$, respectively). The BLAST and SPIRE counts at 250, 350, and 500 μm are globally well reproduced. Nevertheless, the model slightly overpredicts the three last points of Béthermin et al. (2012b) (in red). As discussed by these authors, this could be related to an under-density in GOODS-N. The contribution of lensed sources broadly agrees with the measurements of González-Nuevo et al. (2012) at 350 μm . At 1.1 mm, our model nicely agrees with the combined number counts of Scott et al. (2012)¹⁰, except for the faintest point, originating from 1-2 σ sources and potentially poorly de-biased.

Since the LF evolution and number counts may be degenerate (Béthermin et al. 2012b), galaxy counts split per redshift provide a powerful test of the validity of our model (note that S12 demonstrated that bolometric IR LF are reproduced at $z < 2.5$). This observable is close to the monochromatic LF, but requires fewer corrections (K-corrections, V_{max}) which could bias the results (possible biases from photometric redshifts and source identification are discussed in Berta et al. 2011 and Béthermin et al. 2012b). The comparison between our model and observations (Fig. 4) reveals a good overall agreement between predictions and data. However, we

slightly over-predict the counts around 500 μJy between $z=0.5$ and $z=2$ at 24 μm . It could be due to a slight excess of PAH features around 15 μm in the SB templates. We also underpredict the counts at 100 and 160 μm by 1-2 σ , probably due to a slight lack of warm dust in the SED templates. Finally, our model overpredicts by $\sim 3\sigma$ the $z > 2$ counts in the 2-6 mJy range. As explained in the previous paragraph, this could be due to cosmic variance, as these points rely exclusively on GOODS-N.

By distinguishing between MS and SB activity, the 2SFM framework allows us to explore selection biases toward MS or SB objects in surveys probing various wavelengths and flux density regimes. MS galaxies (dotted line in Fig. 3) dominate the number counts at all flux densities and all wavelengths. However, the relative contribution of SBs varies a lot with flux density and wavelength and is important ($\sim 30\%$) around 30 mJy at 70 μm and 50 mJy at 350 and 500 μm . The relative contribution of SB is very sensitive to the evolution of their SED, which is few constrained. If $\langle U \rangle$ did not evolve with redshift, SBs would dominate around 100 mJy at 350 and 500 μm and at flux densities larger than 8 mJy at 1.1 mm.

Finally, by assuming a non-evolving IR-radio correlation ($q_{TIR} = \log\left(\frac{L_{IR}}{3.75 \times 10^{12} \text{ W}} \times \frac{\text{W Hz}^{-1}}{L_{1.4 \text{ GHz}}}\right) = 2.64$) out to high redshift (e.g. Sargent et al. 2010) and a synchrotron spectral slope $\alpha=0.8$ ($S_{\nu} \propto \nu^{-\alpha}$), we also investigate the contribution of SF galaxies to radio source counts at 1.4 GHz (see Fig. 3). We combined our model for star-forming objects with the model of AGN-driven radio sources of Massardi et al. (2010). The result agrees with the compilation of Vernstrom et al. (2011) (see Fig. 3). According to our model, the 1.4 GHz counts are dominated by SF objects below 200 μJy , in agreement with the observations of e.g. Seymour et al. (2008). We predict the presence of a bump in the Euclidian-normalized radio counts around 40 μJy which is essentially due to MS galaxies.

5. CONCLUSION

Our model based on the main assumption of two SF modes (MS and SB) is able to accurately reproduce the emission of galaxies integrated over most of the Hubble time as probed by galaxy counts from the mid-IR to radio wavelengths. This model contains two main ingredients: the evolution of MS and SB galaxies based on the S12 formalism and a new library of MS and SB SEDs derived from *Herschel* observations (M12). Despite its simplicity, our model provides one of the best fits achieved so far to the number counts, including counts per redshift slice in the SPIRE bands, which were poorly reproduced by the previous generation of models. All these results were obtained without any arbitrary tuning of parameters that are not constrained by observations, contrary to most previous models. The decomposition into 2 modes of SF (2SFM), i.e. MS and SB, associated with two different families of SEDs, is thus a very powerful framework to statistically describe the dust emission of galaxies across cosmic time. In addition, we present a new stochastic AGN treatment, and also found that MS galaxies are responsible for a bump in the 1.4 GHz radio counts around 50 μJy .

This model can be combined with halo models assuming a link between SFR, M_{\star} , and halo mass (e.g. Béthermin et al. 2012a; Wang et al. 2012) to interpret the clustering of

¹⁰ The counts showed in Fig. 3 are corrected for the bias found in their simulation.

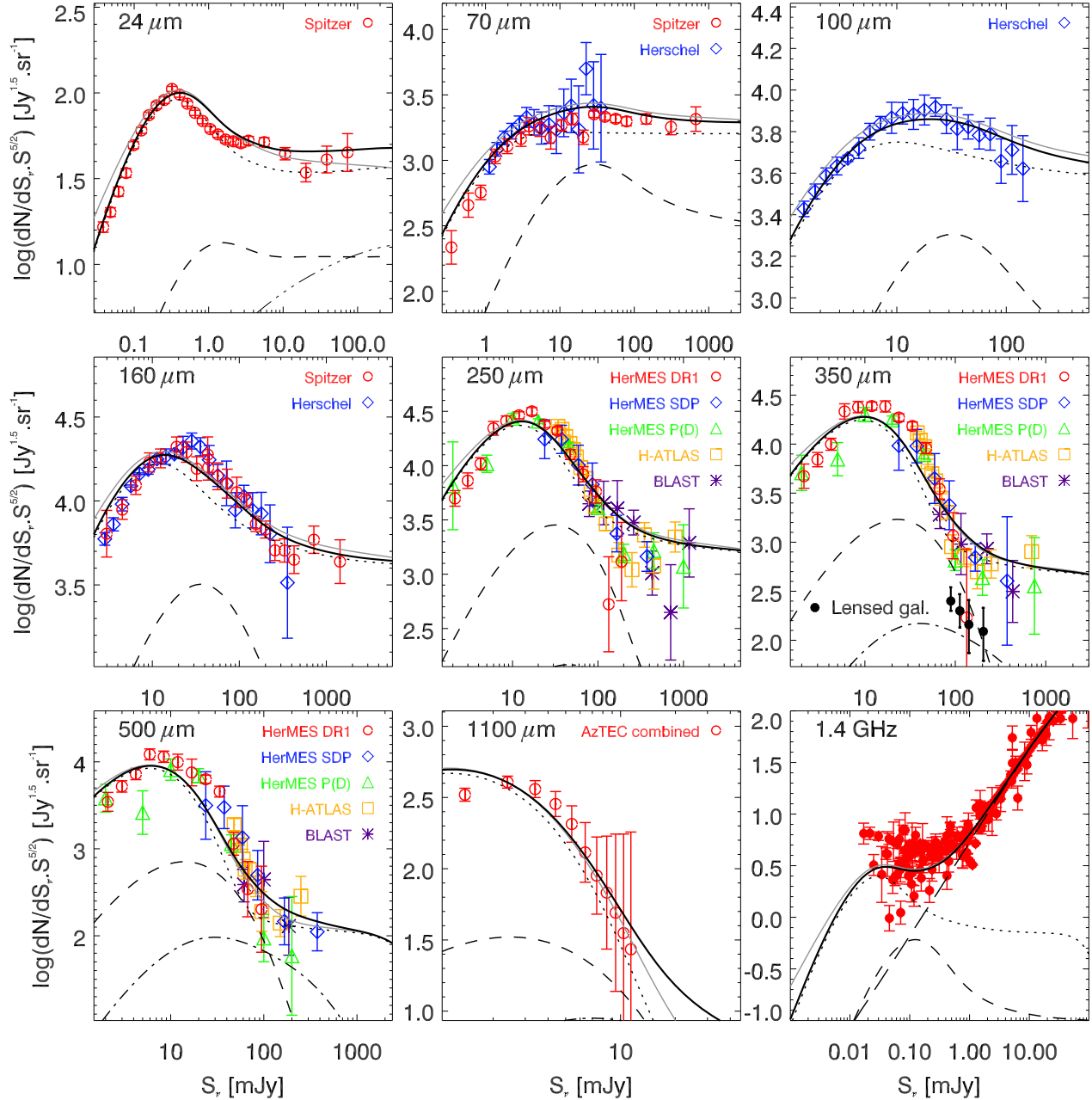


FIG. 3.— Number counts from $24\mu\text{m}$ to 1.4GHz . Solid line—total counts predicted by the model; grey line—counts predicted by the simplified model (without refinements discussed in Sect. 3); dotted line—MS contribution; short-dashed line—SB contribution; dot-dashed line—lensed sources; triple-dot-dashed line—difference between counts with and without AGN contribution. At 1.4GHz , we also plot the model of AGN-driven radio sources of Massardi et al. (2010) (long-dashed line) and combine it with our model of SF galaxies. Data points—B  thermin et al. (2010a) (red points at 24 , 70 , and $160\mu\text{m}$), Berta et al. (2011) (blue points 70 , 100 , and $160\mu\text{m}$), B  thermin et al. (2012b) (red points at 250 , 350 and $500\mu\text{m}$), Oliver et al. (2010) (blue points at 250 , 350 and $500\mu\text{m}$), Glenn et al. (2010) (green points at 250 , 350 and $500\mu\text{m}$), Clements et al. (2010) (yellow points at 250 , 350 and $500\mu\text{m}$), B  thermin et al. (2010b) (purple points at 250 , 350 and $500\mu\text{m}$), Scott et al. (2012) (red points at 1.1mm), and Vernstrom et al. (2011) (compilation of 1.4GHz radio counts). Black dots—contribution of lensed galaxies at $350\mu\text{m}$ measured by Gonz  lez-Nuevo et al. (2012).

infrared galaxies and the fluctuation of the cosmic infrared background (e.g. Planck collaboration et al. 2011). Finally, this model and its future extensions will provide predictions for the next generation of IR, mm, and radio surveys, and, in particular to anticipate which galaxy populations will be preferentially detected, depending on the survey strategy adopted.

We acknowledge Kimberley Scott, Herv   Aussel, Emeric Le Floc’h, Benjamin Magnelli, the anonymous referee, ERC-StG UPGAL 240039, and ANR-08-JCJC-0008.

REFERENCES

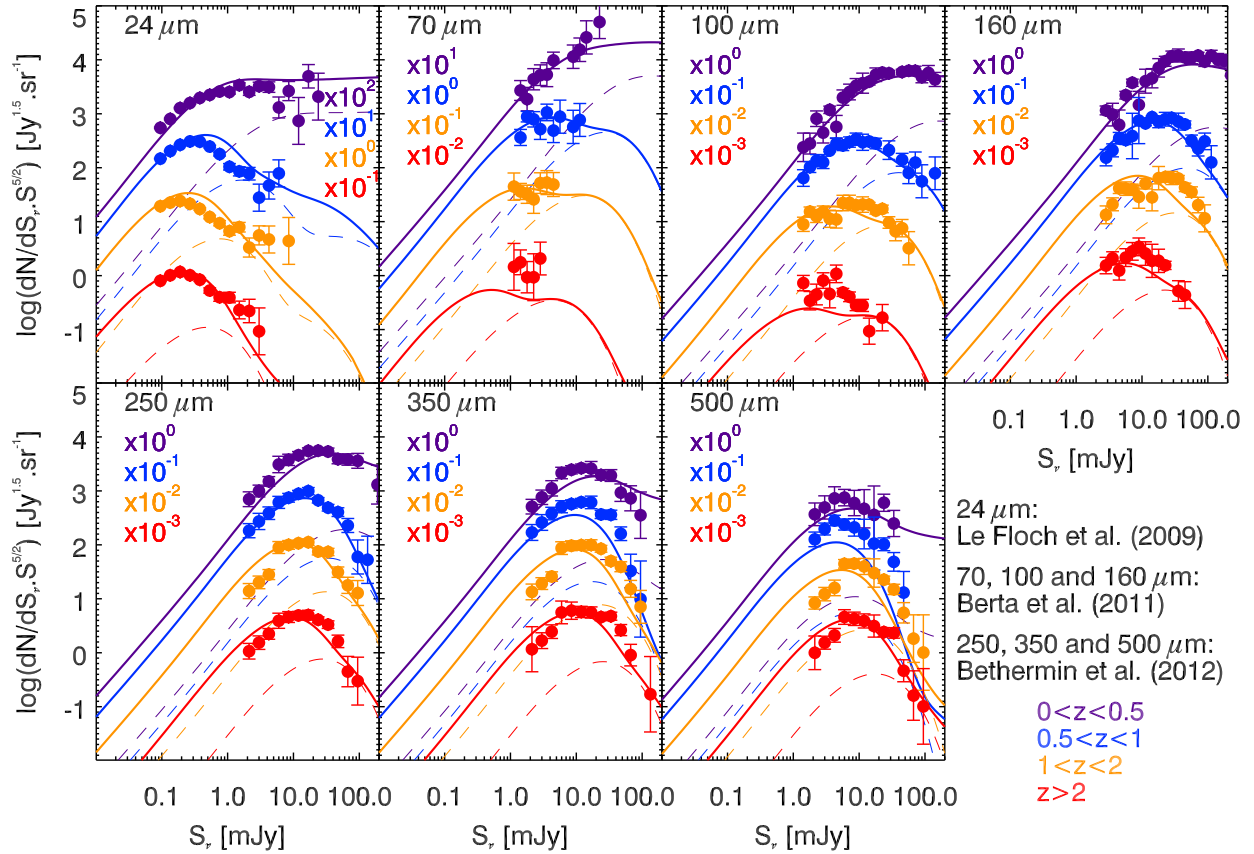


Fig. 4.— Normalized number counts per redshift slice, compared to model predictions. Data from Le Floch et al. (2009) ($24\ \mu\text{m}$), Berta et al. (2011) (70 , 100 , $160\ \mu\text{m}$), and Béthermin et al. (2012b) (250 , 350 , $500\ \mu\text{m}$). For clarity, a redshift-dependent vertical offset has been applied to model and data. Dashed line – contribution of SB.

Béthermin, M., Dole, H., Cousin, M., & Bavouzet, N. 2010b, *A&A*, 516, A43
 Béthermin, M., Dole, H., Lagache, G., Le Borgne, D., & Penin, A. 2011, *A&A*, 529, A4
 Béthermin, M., Doré, O., & Lagache, G. 2012a, *A&A*, 537, L5
 Béthermin, M., Le Floch, E., Ilbert, O., et al. 2012b, *A&A*, 542, A58
 Bouwens, R. J., Illingworth, G. D., Franx, M., & Ford, H. 2007, *ApJ*, 670, 928
 Clements, D. L., Rigby, E., Maddox, S., et al. 2010, *A&A*, 518, L8
 Daddi, E., Dickinson, M., Morrison, G., et al. 2007, *ApJ*, 670, 156
 Draine, B. T. & Li, A. 2007, *ApJ*, 657, 810
 Elbaz, D., Daddi, E., Le Borgne, D., et al. 2007, *A&A*, 468, 33
 Elbaz, D., Dickinson, M., Hwang, H. S., et al. 2011, *A&A*, 533, A119
 Glenn, J., Conley, A., Béthermin, M., et al. 2010, *MNRAS*, 409, 109
 González, V., Labbé, I., Bouwens, R. J., et al. 2010, *ApJ*, 713, 115
 González-Nuevo, J., Lapi, A., Fleuren, S., et al. 2012, *ApJ*, 749, 65
 Gruppioni, C., Pozzi, F., Zamorani, G., & Vignali, C. 2011, *MNRAS*, 416, 70
 Hezaveh, Y. D. & Holder, G. P. 2011, *ApJ*, 734, 52
 Hopkins, P. F., Younger, J. D., Hayward, C. C., Narayanan, D., & Hernquist, L. 2010, *MNRAS*, 402, 1693
 Ilbert, O., Salvato, M., Le Floch, E., et al. 2010, *ApJ*, 709, 644
 Karim, A., Schinnerer, E., Martínez-Sansigre, A., et al. 2011, *ApJ*, 730, 61
 Kennicutt, R. C., Jr. 1998, *ApJ*, 498, 541
 Lacey, C. G., Baugh, C. M., Frenk, C. S., et al. 2010, *MNRAS*, 405, 2
 Lapi, A., González-Nuevo, J., Fan, L., et al. 2011, *ApJ*, 742, 24
 Le Floch, E., Aussel, H., Ilbert, O., et al. 2009, *ApJ*, 703, 222
 Lutz, D., Maiolino, R., Spoon, H. W. W., & Moorwood, A. F. M. 2004, *A&A*, 418, 465

Magdis, G. E., Daddi, E., Béthermin, D., et al. 2012, sub. to *ApJ*
 Magnelli, B., Elbaz, D., Chary, R. R., et al. 2011, *A&A*, 528, A35+
 Massardi, M., Bonaldi, A., Negrello, M., et al. 2010, *MNRAS*, 404, 532
 Mullaney, J. R., Alexander, D. M., Goulding, A. D., & Hickox, R. C. 2011, *MNRAS*, 414, 1082
 Mullaney, J. R., Daddi, E., Béthermin, M., et al. 2012, *ApJ*, 753, L30
 Negrello, M., Hopwood, R., De Zotti, G., et al. 2010, *Science*, 330, 800
 Negrello, M., Perrotta, F., González-Nuevo, J., et al. 2007, *MNRAS*, 377, 1557
 Noeske, K. G., Weiner, B. J., Faber, S. M., et al. 2007, *ApJ*, 660, L43
 Oliver, S. J., Wang, L., Smith, A. J., et al. 2010, *A&A*, 518, L21
 Pannella, M., Carilli, C. L., Daddi, E., et al. 2009, *ApJ*, 698, L116
 Peng, Y.-j., Lilly, S. J., Kováč, K., et al. 2010, *ApJ*, 721, 193
 Planck collaboration et al. 2011, *A&A*, 536, A18
 Rahmati, A. & van der Werf, P. P. 2011, *MNRAS*, 418, 176
 Rodighiero, G., Daddi, E., Baronchelli, I., et al. 2011, *ApJ*, 739, L40
 Salmi, F., Daddi, E., Elbaz, D., et al. 2012, *ApJ*, 754, L14
 Sargent, M. T., Béthermin, M., Daddi, E., & Elbaz, D. 2012, *ApJ*, 747, L31
 Sargent, M. T., Schinnerer, E., Murphy, E., et al. 2010, *ApJS*, 186, 341
 Scott, K. S., Wilson, G. W., Aretxaga, I., et al. 2012, *MNRAS*, 2839
 Seymour, N., Dwelly, T., Moss, D., et al. 2008, *MNRAS*, 386, 1695
 Sobral, D., Best, P. N., Matsuda, Y., et al. 2012, *MNRAS*, 420, 1926
 Somerville, R. S., Gilmore, R. C., Primack, J. R., & Domínguez, A. 2012, *MNRAS*, 2820
 Vasudevan, R. V. & Fabian, A. C. 2007, *MNRAS*, 381, 1235
 Vernstrom, T., Scott, D., & Wall, J. V. 2011, *MNRAS*, 415, 3641
 Wang, L., Farrah, D., Oliver, S. J., et al. 2012, *ArXiv e-prints*